IL NUOVO CIMENTO Vol. 28 C, N. 1 Gennaio-Febbraio 2005
DOI 10.1393/ncc/i2005-10020-x

Physical simulations of neutral boundary layer in rotating tank

E. Ferrero([1]), A. Longhetto([2]), L. Montabone([3]), L. Mortarini([2])
M. Manfrin([2]), J. Sommeria([4]), H. Didelle([4]), C. Giraud([5]) and U. Rizza([6])

([1]) *Dipartimento di Scienze e Tecnologie Avanzate, Università del Piemonte Orientale Alessandria, Italy*
([2]) *Dipartimento di Fisica Generale, Università di Torino - Torino, Italy*
([3]) *Department of Physics, Oxford University - Oxford, UK*
([4]) *Laboratoire LEGI-Coriolis, CNRS - Grenoble, France*
([5]) *IFSI-CNR - Torino, Italy*
([6]) *ISAC-CNR - Lecce, Italy*

(ricevuto il 24 Febbraio 2005; approvato il 22 Marzo 2005)

Summary. — Laboratory measurements of neutral atmospheric boundary layer (ABL) are presented. The experiment was carried out in the large rotating tank of the Coriolis-LEGI laboratory in Grenoble. An ABL was created at reduced scale and measured. The mean flow was generated, both increasing (spin-up) and decreasing (spin-down) the rotation speed of the platform. Preliminary measurements by acoustic probes were used to assess the decay with time of the flow velocity at the position where turbulence measurements were subsequently performed. The mean velocity and the turbulence fields were then measured by using PIV (Particle Image Velocimetry) technique, which allows to obtain high-resolution measurements in the simulated ABL. For each rotation period and velocity conditions, two vertical cross-sections of the flow were measured at different times, then 3D velocity fields were reconstructed from the two planar fields under convenient geometric (orthogonal) and physical assumptions (reproducibility of the flow). The aim of this work is to collect a useful data set for testing and comparing turbulence models and parameterisations. For this reason, particular attention was paid to the turbulence statistics, turbulent fluxes and scales. The results of the data analysis are presented and discussed.

PACS 92.60.Fm – Boundary layer structure and processes.
PACS 92.10.Lq – Turbulence and diffusion.
PACS 92.60.Ek – Convection, turbulence, and diffusion.

1. – Introduction

It is well known today that in order to understand how irregularities of the ground surface can distort the mean and turbulent structure of the flow and thus to obtain a com-

© Società Italiana di Fisica

plete picture of its structure, it is necessary to solve a full set of fluid dynamics equations using finite differences or more sophisticated numerical methods (see for instance [1, 2]).

The fundamental role played by the higher order turbulence moments in reproducing the turbulent transport not only in complex terrain and convective conditions but also in the neutral horizontally homogeneous conditions, has been recently demonstrated by [2].

On the other hand, the characteristics of the simulated turbulence depend very sensitively on the closure scheme which is adopted. Simple schemes, such as mixing-length model, which are essentially local in nature, are adequate only if there is a near equilibrium between local production and dissipation rates of turbulent kinetic energy. Otherwise non-equilibrium effects become significant and thus a realistic description of the turbulence structure requires considerably more sophisticated closure [3]. A simple model in which the eddy exchange coefficient does not take into account horizontal variations would not be able, in principle, to simulate flows over irregular terrain. Only the introduction of transport equations allows to account for such inhomogeneities.

For these reasons, the assessment of turbulent fluxes of momentum and wind field in the atmospheric boundary layer is a topic of great interest from both a theoretical and practical point of view and still an open problem.

One of the main problems in developing turbulence models is to find a complete data-set for determining parameterisations and empirical constants and for comparing the model results. These data-sets are difficult to obtain in open-field experiments because of the uncontrolled flow conditions. Useful data can be gathered in wind tunnel experiments, but these cannot take into account the Earth rotation [4, 5]. Recently LES was adopted in literature as a base for comparison of other models and parameterisations [6, 7].

In this work a method for obtaining detailed observations of a rotating neutral boundary layer from laboratory experiments carried out under controlled conditions is presented. In order to assess the reliability of the method, a few simple schematic examples of ABLs over both smooth and rough flat surfaces have been selected. The laboratory facilities and measurement methodologies are illustrated and the results in terms of turbulence moments and diffusion coefficient are shown.

2. – The laboratory experiment

This work consists in a series of laboratory simulations of the dynamics of a rotating neutral turbulent ABL and their influence on the diffusive conditions of the atmosphere.

The laboratory experiments took place on the hydrodynamic rotating tank of "Coriolis/LEGI" (Grenoble). The rotating speed of the tank can be continuously changed up to 5 revolutions per minute, allowing to achieve Rossby numbers typical of mesoscale circulations ($10^{-1} < \mathrm{Ro} < 1$). The large platform of "Coriolis/LEGI" laboratory is essential for getting the above-mentioned results not only on account of the horizontal spatial scale, but mainly because it allows the necessary resolution for reproducing the surface roughness elements and for determining the velocity field inside the topographical features of the simulated complex terrain.

The LASER-PIV (Particle Image Velocimetry) system, annexed to this hydrodynamic simulation laboratory, allows the quantitative measurement of fluctuating velocity fields. This can be accomplished by seeding the water with particles (60 μm in diameter), illuminating it with a light sheet produced by a continuous Argon laser equipped with a beam expanding optical device. A high-resolution numerical CCD camera records sequences of images shot at adjustable time rates and a dedicated software identifies the displacement of clusters of particles by means of cross-correlation technique between

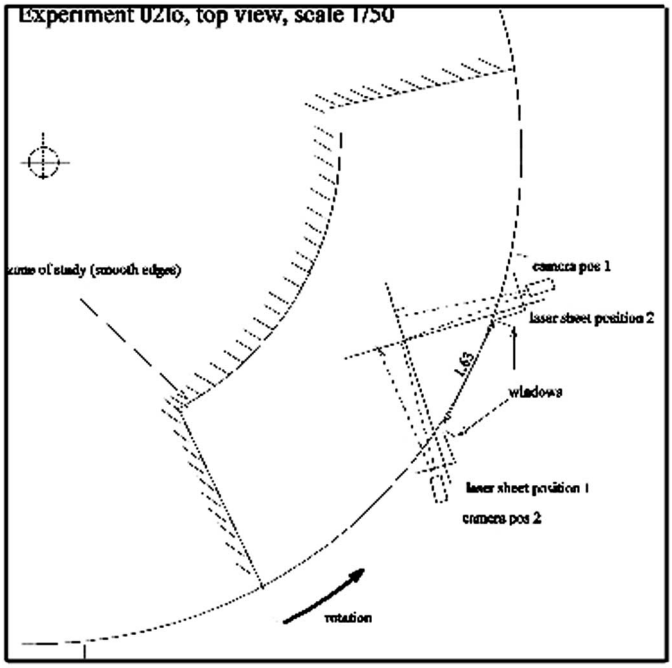

Fig. 1. – Experimental set-up.

pairs of images. The velocity of the flow at any point of the measured region [8] is then calculated at each time.

A schematic picture of the experiment layout is shown in fig. 1. Two different configurations of the camera and the light sheet were used to get two horizontal components of the flow. These components were subsequently composed to reconstract the full 3D velocity field.

The experiments were carried out with different values of the roughness length. In the first case no roughness elements were put in the tank, while in the second series of experiments cubic-shaped elements were glued to the tank bottom.

The mean flow $U(r)$ at the distance r from the center of the tank was created either by increasing (spin–up) or by decreasing (spin-down) the tank rotation speed. The initial velocity of the flow was controlled by choosing different values for the initial (T_0) and final (T_1) rotation periods.

The turbulent equilibrium boundary layer depth can be evaluated as

$$\delta_t = 0.4\frac{u_*}{f}\,, \tag{1}$$

where $f = 4\pi/T_1$.

The frictional velocity was evaluated by the following empirical formula [9]:

$$u_* = \alpha u_\infty\,, \tag{2}$$

where u_∞ is the free stream velocity outside the turbulent layer and the coefficient

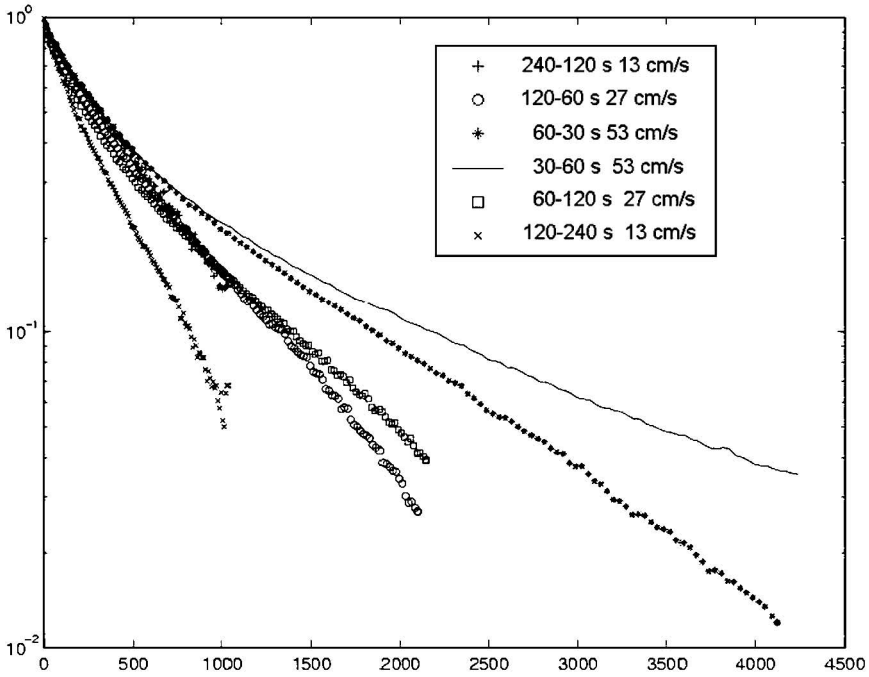

Fig. 2. – Normalised velocity as a function of the normalised time.

$\alpha = 0.07$ was estimated, in a previous work [9], from the velocity measurements performed with a total water depth of 30 cm and different spin-up and spin-down conditions. It can be noted that the free stream velocity in the tank plays the role of the geostrophic wind in the actual atmosphere.

Considering that $U = 2\pi(1/T_1 - 1/T_0)r$, we have

$$\delta_t = 0.2\alpha \left(1 - \frac{T_1}{T_0}\right) r \tag{3}$$

which does not depend on the rotation period.

Since in all the experiments we have $T_1/T_0 = 1/2$ and $r = 5.1$ m, we expect

$$\delta_t = 3.6\,\mathrm{cm}\,. \tag{4}$$

On the other hand, the Reynolds number based on the laminar depth is

$$\mathrm{Re}_l = \frac{U\delta}{\nu} = \left(1 - \frac{T_1}{T_0}\right) r\,(2\pi)^{1/2}\,(\nu T_1)^{-1/2} = 6390\,T_1^{-1/2}\,, \tag{5}$$

where

$$\delta = \left(\frac{\nu T_1}{2\pi}\right)^{1/2}\,. \tag{6}$$

It may be useful to recall that the Ekman layer instability is attained for Re_1 of the order of 55. Hence, turbulence is fully developed for Reynolds numbers higher than this value.

In the experiments with values of T_1 ranging from 30 s to 240 s we obtained Reynolds numbers ranging from 412 to 1166. These values refer to the initial velocity; during the experiment the velocity decreases, due to the viscous forces acting on the system, and the Reynolds numbers lower. The flow, initially turbulent, after about 10^2 normalised times becomes laminar, as can be seen in fig. 2, where the normalised velocity U/U_0 (U_0 being the initial velocity after the spin-up or spin-down), measured by acoustic probes in the bulk of the flow, is depicted as a function of the normalised time, tU_0/H (where $H = 30$ cm is the total depth of the fluid in the preliminary tests). It can be observed that the slopes of the curves change at this time indicating the different regimes of the two intervals. However, a turbulent boundary layer was generated close to the wall also for normalised times greater than 10^2.

3. – Data preprocessing and processing

For each view of the flow, as explained above, the experiments have produced a time series of 714 raw images of the fluid uniformly seeded with particles. Cross-correlation between a pair of images is used to obtain the displacements of patches of particles over a sufficiently small time interval, a technique known as Particle Image Velocimetry (PIV) or Digital Particle Image Velocimetry (DPIV). See [10] for a complete review of the bases of this technique, although it does not include recent developments and improvements.

Before using PIV, raw images have been preprocessed to eliminate a very bright line which corresponds to the illumination of the particles settled down on the tank floor. We performed an average (pixel by pixel) over the whole series of 714 images and then removed, from each image, only the part close to the floor with a weighed subtraction.

The Correlation Image Velocimetry (CIV) algorithm by [11] is used to obtain the 2D velocity vectors on a planar grid. This state-of-the-art algorithm incorporates advanced features (such as the multi-passage option) which improve the performance and allow for obtaining accurate values for the velocities; see [8, 11] for details. Two versions of CIV (CIV1 and CIV2) have been developed. The more advanced algorithm corresponds to CIV2, while CIV1 is rather standard. For the purpose of these experiments, we have mainly used the on-line correlation peak averaging of Hart for reducing the number of wrong vectors, together with a post-processing outliers detection and filtering algorithm based on the low correlation value of an interrogate vector. The quality of most of the raw images after the preprocessing was such to use a rectangular interrogation window of 30×20 pixels, obtaining a final resolution of about 60×80 vectors on the grid (the exact numbers vary slightly in the different experiments, due to different camera view fields).

Each experiment includes two time series of 714 raw images of the fluid taken at an angle of 45 degrees with respect to the direction of the flow, as explained above. These time series span about 12 seconds at a frequency of 60 Hz, and for most experiments consecutive images have been used for cross-correlation, so that velocity fields are available at the same frequency.

4. – PIV measurements analysis

As said before, for each flow condition we measured two planar fields on two vertical orthogonal cross-sections. From them, we reconstruct 3D flow fields, assuming statistical reproductibility of the flow. The streamwise (azimuthal) and crosswise (radial) velocity components, u and v, respectively, are obtained from the horizontal velocity components u_1 and u_2, measured with each camera

$$u = (\sqrt{2}/2)(u_1 + u_2)\,, \qquad v = (\sqrt{2}/2)(u_1 - u_2)\,. \tag{7}$$

The wall is visible in each image, and the apparent vertical is defined as the direction perpendicular to this wall (it is nearly aligned with the image y-axis). In reality the apparent vertical particle displacement is a projection in the field of view, which is slightly tilted with respect to the true vertical (see fig. 3). The local tilt angle at height z from the wall is $(z - z_c)/L$, where $z_c = 15$ cm is the camera height above the tank floor and $L = 200$ cm the distance between the camera and the field of view. Using the approximation of a small angle, the true vertical velocity w is related to the apparent vertical velocities w_1 and w_2 seen by the camera 1 and 2, respectively, by the geometric projections:

$$w = w_1 - (z - z_c)u_2/L\,, \qquad w = w_2 + (z - z_c)u_1/L\,. \tag{8}$$

The time-averaged velocity components $\langle u\rangle$, $\langle v\rangle$, $\langle w\rangle$ are obtained by applying the time averaging operator to (7) and (8) taken at the same height z. The mean vertical velocity $\langle w\rangle$ is then obtained twice by each of the cameras, and we take as the final result the average of the two values.

Multiplying the two relations (8) by u_1 and u_2 respectively before averaging, we get

$$\langle wu_1\rangle = \langle w_1u_1\rangle - (z - z_c)\langle u_1u_2\rangle/L\,, \qquad \langle wu_2\rangle = \langle w_2u_2\rangle + (z - z_c)\langle u_1u_2\rangle/L\,. \tag{9}$$

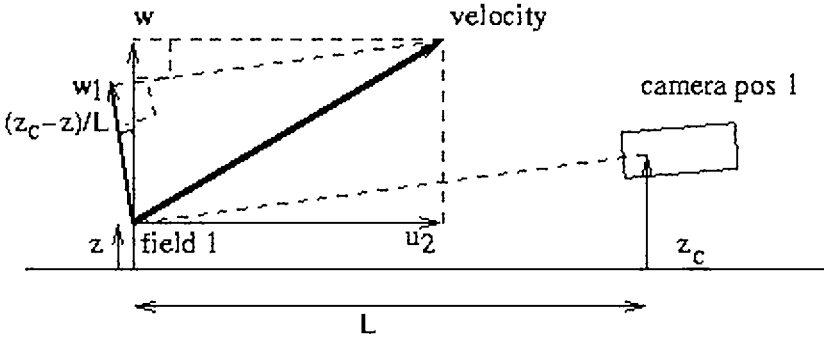

Fig. 3. – Parallax correction.

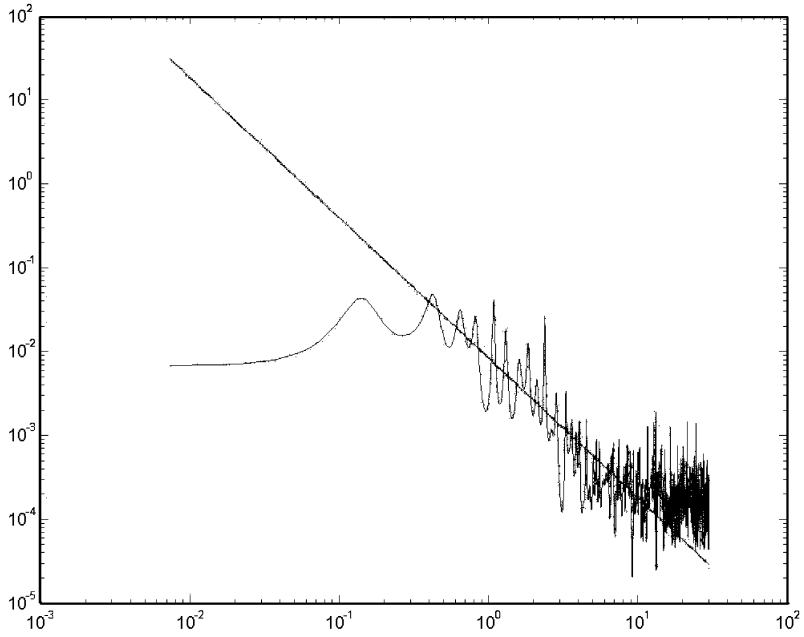

Fig. 4. – Power spectrum (σ_w^2/f) as a function of the frequencies (f). The line represents the $f^{-5/3}$ behaviour in the inertial subrange.

Adding these two relations, we get the streamwise (azimuthal) Reynolds stress (the parallax corrections in $\langle u_1 u_2 \rangle$ cancel each other)

$$\langle wu \rangle = (\sqrt{2}/2)(\langle w_1 u_1 \rangle + \langle w_2 u_2 \rangle)\,. \tag{10}$$

Note that this method does not apply for the transverse Reynolds stress $\langle wv \rangle$: the parallax corrections in $\langle u_1 u_2 \rangle$ would then add up, and the correlation $\langle u_1 u_2 \rangle$ cannot be obtained by our method, since the two components u_1 and u_2 are not measured simultaneously.

In fig. 4 an example of the power spectrum obtained in the case of the experiment with $U = 4.6$ cm/s and no roughness, at the level $n = 10$ is shown (inside the boundary layer). The turbulence layer appears to be well developed and a two-decades inertial sub-range regime can be observed. This result allows to analyse the boundary layer and to compare it with the case of the atmosphere.

In order to plot the vertical profiles in non-dimensional coordinates and comparing the different experiments, we should evaluate the boundary layer height and the friction velocity.

The boundary layer height z_i can be deduced as the level where the turbulent kinetic energy (TKE) vanishes. The TKE is defined as

$$\begin{aligned} \mathrm{TKE} &= \frac{1}{2}\left(\langle u'^2 \rangle + \langle v'^2 \rangle + \langle w'^2 \rangle\right) \simeq \\ &\simeq \frac{1}{2}\left(\langle u'^2_1 \rangle + \langle u'^2{}_1 \rangle + \frac{1}{2}(\langle w'^2_1 \rangle + \langle w'^2_2 \rangle)\right) \end{aligned} \tag{11}$$

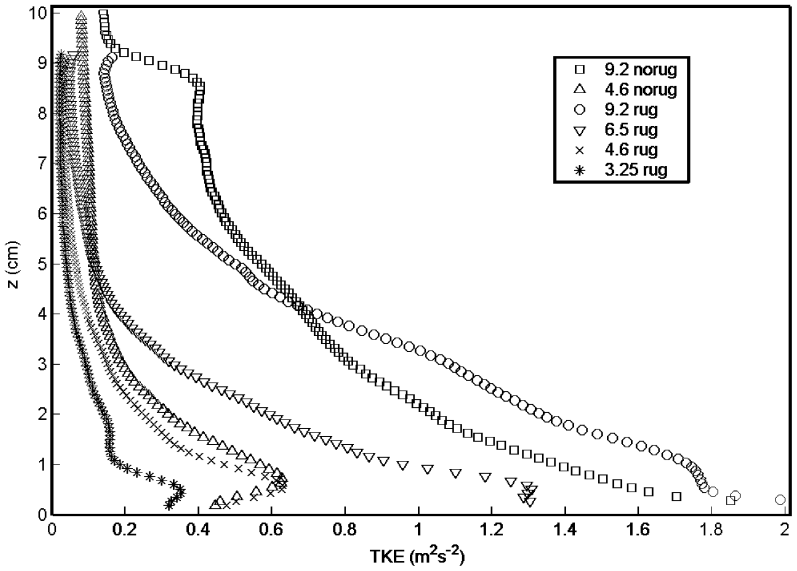

Fig. 5. – Turbulent kinetic energy vertical profile.

(here $u_i' = u_i - \langle u_i \rangle$). For this quantity, we can neglect the parallax corrections (8) to an excellent approximation and for $\langle {w'}^2 \rangle$ we just take the average from the two cameras.

In fig. 5 the vertical TKE profiles corresponding to the six experiments considered are depicted. The boundary layer height z_i was evaluated from these profiles considering the level at which the profiles attain zero. From the vertical profiles the free stream velocity was also estimated for the six experiments and the friction velocities were finally determined from (2). In table I the estimated parameters for each experiment are sumarised.

Figures 6 and 7 show the vertical profiles of $\langle u \rangle$ and $\langle v \rangle$ velocity components made non-dimensional by using the above-estimated parameters. It can be observed that, as expected, the curves corresponding to different runs tend to collapse on the same profile, demonstrating the correctness of the estimation of the surface layer parameters.

We can conclude that the non-dimensional parameters, u_* and z_i, calculated as described above, are the characteristic parameters for the simulated flows.

Concerning the $\langle w \rangle$ components (fig. 8), it can be noted that they were not equal

TABLE I. – *Estimated parameters*

Experiments	U (cm/s)	$u_\star$ (cm/s)	z_i (cm)	T_0	T_1
norug92	10.67	0.74	9.	240	120
norug46	5.95	0.42	8.	240	120
rug92	11.20	0.78	9.	240	120
rug65	7.80	0.55	8.	240	120
rug46	5.65	0.4	8.	240	120
rug325	4.50	0.31	7.	240	120

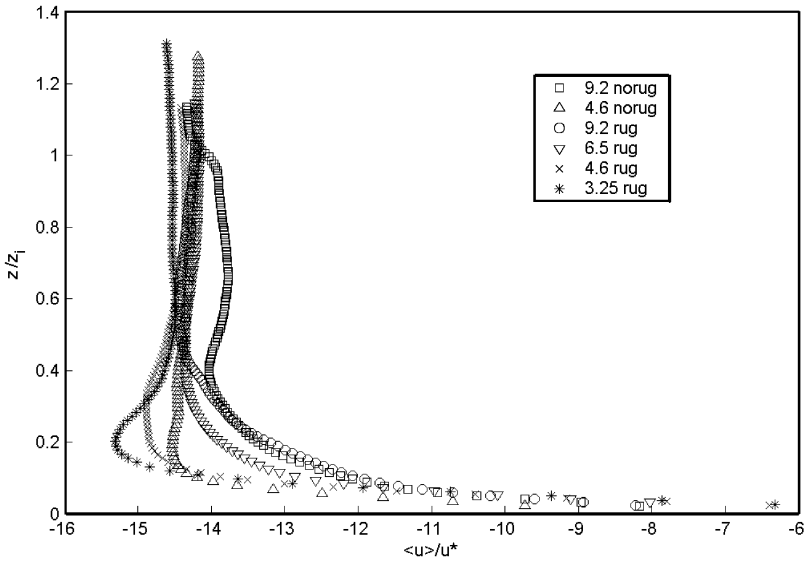

Fig. 6. – Normalised u vertical profiles.

to zero, as it should be over a flat boundary; this could be due to the Ekman pumping generation by the tank rotation.

For the sake of comparison, together with the experimental results we also reported the profiles predicted by two Large Eddy Simulations (LESs).

LES model [7] utilises the incompressible Boussinesq form of the Navier-Stokes equations and considers a horizontally homogeneous boundary layer. The ABL variables

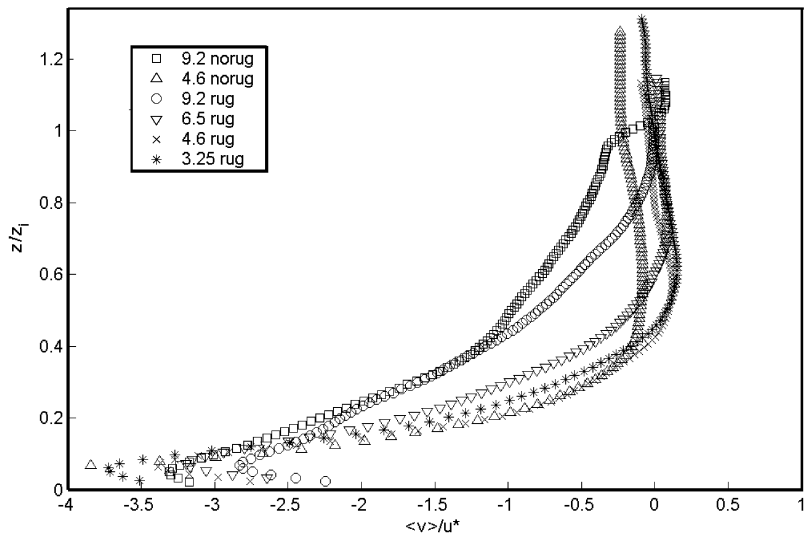

Fig. 7. – Normalised v vertical profiles.

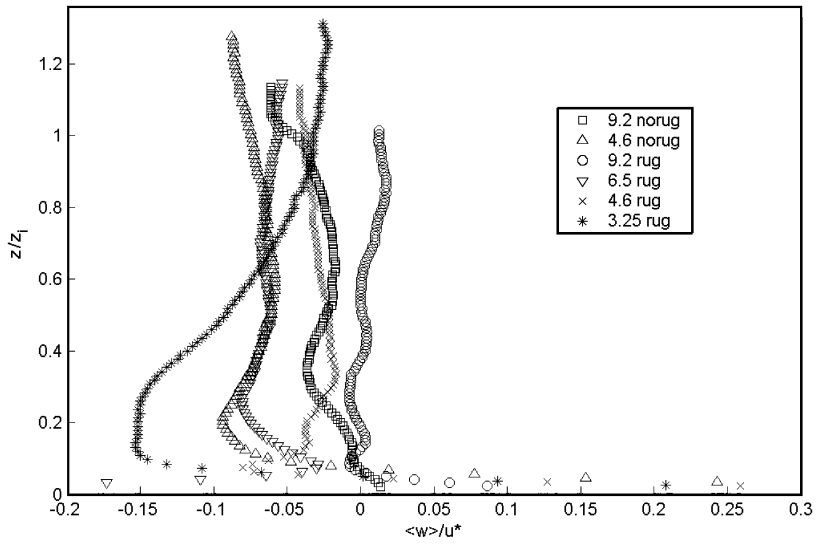

Fig. 8. – Normalised w vertical profiles.

$(u, v, w,$ pressure, temperature, etc. ...) are spatially filtered to define resolved component and sub-grid scale (SGS) component. The filter width is of order of the numerical grid dimension and lies in the inertial subrange of scales in the turbulence spectrum. In the model [6] the SGS energy is found from a prognostic equation [12], while the SGS fluxes are obtained from a first-order closure or flux-gradient relationship. The stress tensor is given by

$$\tau_{ij} = -2\nu_t S_{ij} \,, \tag{12}$$

where the deformation tensor S_{ij} is defined as

$$S_{ij} = \frac{1}{2}\left(\frac{\partial u_i}{\partial x_j} + \frac{\partial u_j}{\partial x_i}\right) . \tag{13}$$

The eddy viscosity ν_t is parameterized as

$$\nu_t = C_k l e_s^{1/2} \,, \tag{14}$$

where C_k is a constant ($\simeq 0.1$), l is a mixing length, e_s is the SGS TKE and its dissipation rate is given by

$$\epsilon = C_\epsilon \frac{e_s^{3/2}}{l} \,, \tag{15}$$

where $C_\epsilon = 0.93$.

In fig. 9 the comparison of the normalised measured and simulated TKE has been shown.

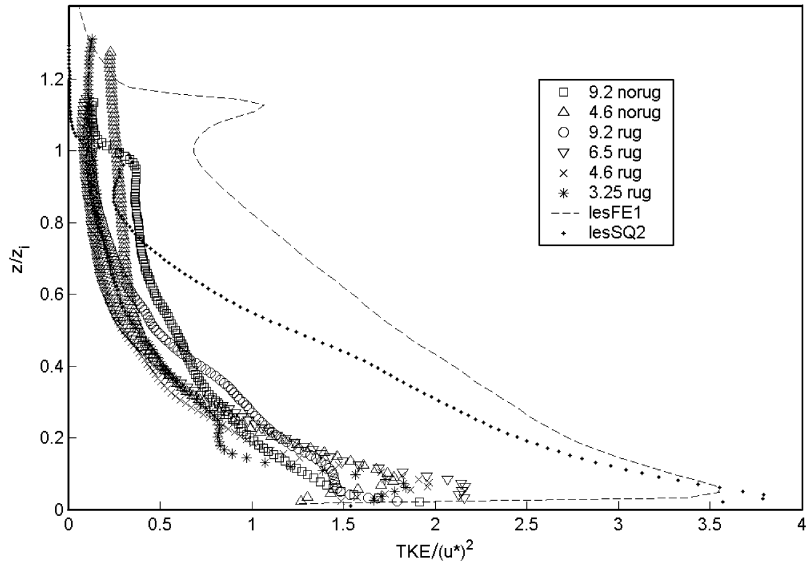

Fig. 9. – Normalised turbulent kinetic energy vertical profiles compared with LES data.

In this work we reproduce by the LES two neutral ABL utilising the same procedure already described by [6], that is first generating a mixed (sheared and convective) ABL, then setting surface heat flux to zero. They are characterised by (LESFE1) U_∞ = 15 m/s, $u_\star$ = 0.5 m/s, z_i = 478 m and (LESSQ2) U_∞ = 15 m/s, $u_\star$ = 0.58 m/s, z_i = 1574 m, respectively. Figure 9 shows that the experimental results underestimate the simulated values of about a factor two.

In fig. 10 the vertical profile of the $\langle u'w' \rangle$ momentum fluxes is shown. Also in this case the experimental results underestimate the LES data, with a different degree as greater as the velocity is smaller.

5. – Diffusion coefficients

When a dispersion process is considered over large vertical scales covering not only the inner and outer ABL but also the lower free atmosphere over an extended horizontal fetch, numerical atmospheric models incorporating turbulent diffusion processes are required in order to describe the diffusion and transport of airborne tracers ([13], pp. 386-389). This means that it is often necessary to be able to approximate the surface stress and fluxes in terms of mean variables at the grid points in the above-mentioned numerical models. Unfortunately, in some models the lowest grid point is well above the surface layer, making it impossible to use flux-profile relationships based on the non-local, Surface Layer Monin-Obukov similarity theory. However, a different similarity theory, the Surface Rossby Number Similarity, built on the matching of surface layer profiles to the external forcing given by flows in the mid boundary layer, can permit that surface stress and fluxes be related to conditions higher in the ABL in terms of mean variables at their grid points ([13], p. 359), [14, 15].

It is then possible to match the flow at the bottom of the mid-ABL with that at the top of the surface layer and relate the surface stress to the mean flow higher in the

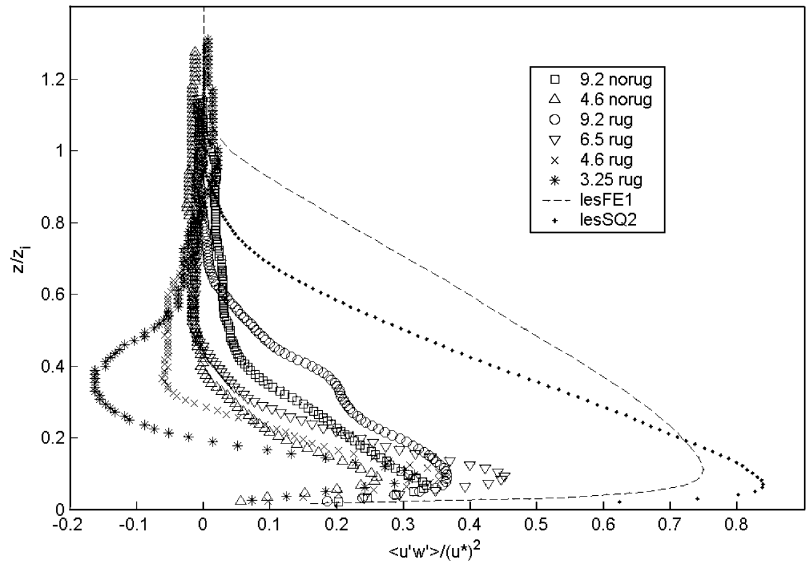

Fig. 10. – Normalised vertical profiles of the $\langle u'w' \rangle$ compared with LES data.

interior of the ABL, giving the bulk transfer, or drag coefficients, which allow one to find the surface flux given knowledge of mean variables aloft and at the surface ([13], p. 387). In fact, when we have the bulk transfer, or drag coefficient $[CD = V^2/u_*^2]$, we can use the following relationships, parameterised by many authors [16-19] to obtain surface fluxes Φ_ϵ of a property ϵ ([13], p. 270):

$$\Phi_\epsilon = -C_\mathrm{g} V_\mathrm{g} [\epsilon_\mathrm{top} - \epsilon_\mathrm{bottom}] \,, \tag{16}$$

where C_g is called the geostrophic drag coefficient and V_g is the magnitude of the geostrophic wind. Here the geostrophic wind and then the geostrophic drag coefficient are used, because sometimes in numerical or theoretical models one does not know the winds anywhere near the surface, but one can calculate the geostrophic wind instead [13], p. 270.

In the particular event of the geostrophic drag coefficient C_GN for neutral atmospheric conditions, the following parameterisation has been suggested:

$$C_\mathrm{GN} = 0.0123 \, \mathrm{Ro}_0^{-0.14} \,, \tag{17}$$

where $\mathrm{Ro}_0 = V_\mathrm{g}/f z_0$ represents the surface Rossby number. This number differs from the Rossby number Ro based on the mesoscale scales for the lengths and velocities.

The main problem to deal with now is to look for the set of scales that produce the correct non-dimensionalization of the ABL equations, that is guarantee the Surface Rossby Number Similarity, assuring that everything becomes independent of the external parameters, in particular the non-dimensional vertical profiles of the most relevant turbulent parameters, such as the turbulent diffusion coefficient, the dissipation rate of turbulent kinetic energy, the vertical temperature gradient, and so on. As the geostrophic wind can be calculated quite easily, equations expressing the matching between the bottom

and higher ABLs through this scale velocity, also known as geostrophic drag laws, have attracted particular interest in the community of ABL physicists. It has been demonstrated by [20] that the Surface Rossby-number similarity condition in the ABL exists above a height $Z_R = Z_0$, where Z_R and Z_0 are the normalised (standardised) vertical height and roughness length, respectively, if the relevant physical quantities of the ABL are made dimensionless with the following internal scales:

$$\text{friction velocity} \quad u_* \tag{18}$$

$$\text{internal scale height} \quad h = ku_*/f\,. \tag{19}$$

It can be noted that h is the turbulent boundary layer depth δ_t already defined (eq. (1)) and, in general may not coincide with the experimental value z_i listed in table I. With these internal scales, it is possible to define the following reduced (non-dimensionalized) variables with internal parameters:

$$Z = \frac{z}{h}\,, \tag{20}$$

$$K_m = \frac{k_m}{h^2 f} = \frac{k_m}{ku_*^2/f}\,, \tag{21}$$

$$(U, V) = k\frac{u, v}{u_*}\,, \tag{22}$$

$$(T_x, T_y) = \frac{(\tau_x, \tau_y)}{\rho u_*^2}\,, \tag{23}$$

where K_m is the reduced turbulent diffusion coefficient, (U, V) are the reduced x and y wind speed components, (T_x, T_y) are the reduced turbulent stress component and k is the von Karman constant. By using Prandtl's mixing length relation

$$k_m = \ell^2 \left|\frac{\mathrm{d}v}{\mathrm{d}z}\right|, \tag{24}$$

where ℓ is the mixing length, a new expression can be obtained for the reduced K_m. We obtain first

$$K_m = L^2 \left|\frac{\mathrm{d}V}{\mathrm{d}Z}\right| \frac{1}{k^2}\,, \tag{25}$$

where $L = \ell/h = \ell f/(ku_*)$ is the reduced mixing length non-dimensionalized with internal parameters. Then, by recalling the flux-gradient relationship $(\tau_x, \tau_y) = \rho k_m \mathrm{d}(u, v)/\mathrm{d}z$, one can obtain $k_m = l(\tau/\rho)^{1/2}$ or, in reduced form,

$$K_m = \frac{L}{k}(T_x^2 + T_y^2)^{1/4}\,. \tag{26}$$

If the orientation of the x-axis of the coordinate system is chosen along the direction of the surface stress τ_0 (rather than the surface geostrophic wind $V_{\mathrm{g}0}$) and reduced variables non-dimensionalized only with internal parameters are used, in [20] it is demonstrated that the equations of the ABL, as well as their boundary conditions, are independent of any external parameters for $Z \geq Z_R$ (Surface Rossby Number Similarity). More

precisely, they also demonstrated that this property, that holds true for almost all of the quantities defining the structure of a rotating turbulent ABL, does not apply for the profiles of K_m. In fact, in the chosen coordinate system (where $T_x = T_{x0}, T_y = 0$), the non-dimensional mixing-length hypothesis reads as $L_0 = kZ_0$ at $z = z_0$, and eq. (25) will become (again at $z = z_0$): $K_{m0} = Z_0$ and hence

$$K_{m0} = L_0/k$$

or, in dimensional form,

$$k_{m0} = ku_* z_0$$

which is the well-known Prandtl mixing-length hypothesis for $z = z_0$, assuring a perfect coincidence of the different K_m profiles in the lowest part of the ABL.

This is not the same if we use reduced variables non-dimensionalized with external parameters, because in this case the equations of the ABL depend on external parameters which contain internal as well as external parameters. When conditions of Surface Rossby Number Similarity apply, reduced vertical profiles of $T_x(Z)$, $T_y(Z)$ and $K_m(Z)$ in barotropic ABLs are universal functions, valid for arbitrary external parameters. The experiments carried out in the Coriolis tank offered a special opportunity to test the validity of the approximation of the above law.

In figs. 11 a and b the momentum diffusion coefficient K_m vertical profiles,

$$K_m = -\frac{\langle u'w' \rangle}{\mathrm{d}U/\mathrm{d}z} \tag{27}$$

for the different experiments are depicted in dimensional and non-dimensional coordinates.

In order to make the vertical coordinate non-dimensional, we use the experimental ABL height z_i.

As has been explained before, the different experiments have been carried out with two different roughness conditions. The lowest one corresponded to the roughness of the floor of the tank, which was quite smooth; the second one corresponded to roughness created on the tank floor by gluing on it a large number of small cubes whose sides were $l_c = 4 \times 10^{-3}$ m, almost randomly distributed with a mean distance of 8×10^{-2} m in order to avoid regular and stationary streamlines at the bottom of the water flow. This distribution of cubes produced an equivalent roughness $z_0 \sim 10^{-1} l_c$, corresponding to a dimensionless roughness $Z_0 = 5 \times 10^{-3}$, considering a turbulent boundary layer depth equal to 8×10^{-2} m.

According to the previous theoretical development, the surface Rossby number similarity should exist everywhere in the ABL above a height $Z_\mathrm{g} \geq 10 Z_0$, where the vertical profiles of all physical quantities should collapse on a unique, universal profile, except for the reduced turbulent diffusion coefficient K_m when a relationship, expressing the mixing-length hypothesis, is introduced. In which case, the surface Rossby number similarity should exist for $Z_\mathrm{g} \geq Z_0$.

However, our normalised K_m profiles seem to violate this second theoretical expectation, and to comply rather with the first and more general property, according to which surface-Rossby number similarity appears only above the reduced height $Z_R \geq 10\, Z_0$.

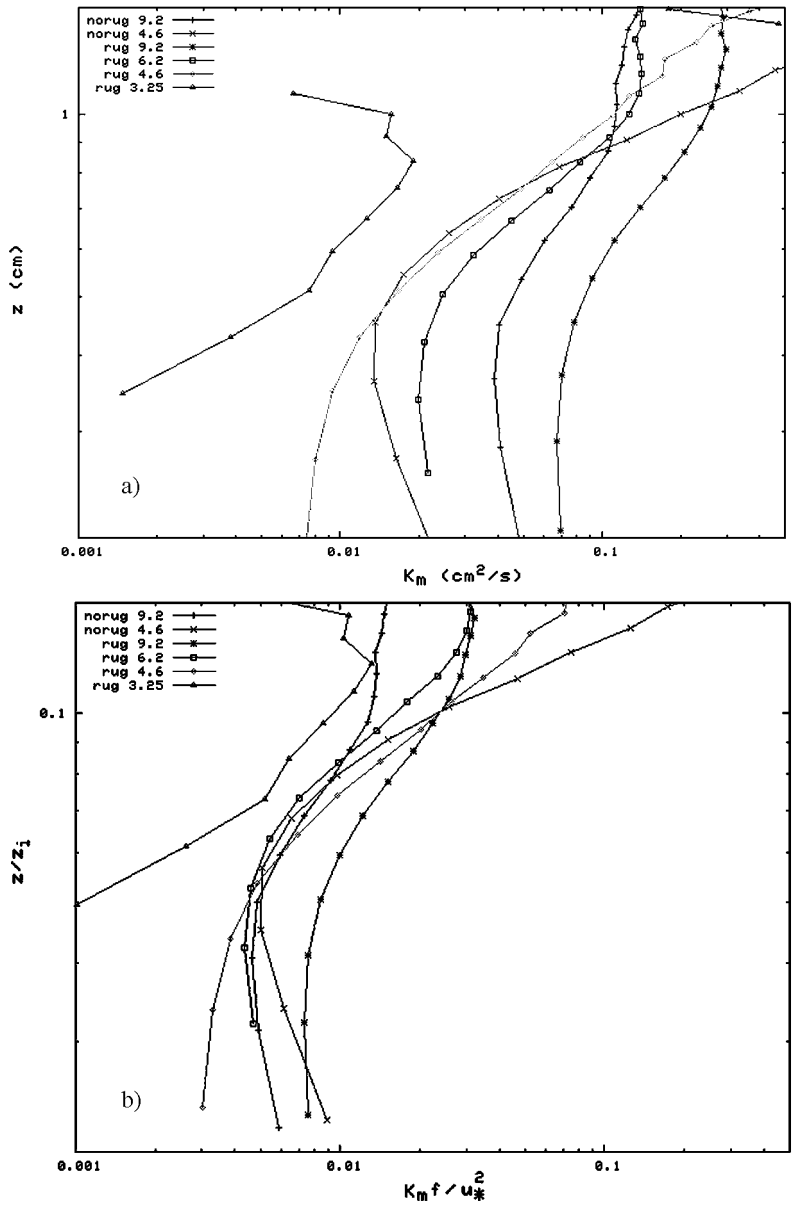

Fig. 11. – Diffusion coefficient (a), normalised diffusion coefficient (b).

As a matter of fact, the dimensionless profiles collapse into a unique profile in the layer between $Z = 0.05$ and $Z = 0.1$ (fig. 11b).

Concerning the cases without roughness, it can be observed that the two dimensionless profiles match at a lowest level of the range where the Rossby number similarity applies ($Z = 0.05$).

One explanation of this departure from the theoretical expectation could be that

the turbulence developed near the bottom of the water layer in the rotating tank was not similar to the homogeneous, small-scale turbulence assumed by the mixing-length assumption for the lower layers of the atmospheric ABL. This explanation is suggested by the fact that considerable doubt has been long since thrown on the fundamental assumption that the shearing stress in a boundary layer is directly related to the gradient of mean velocity. On the other hand, the Prandtl-mixing length theory appears to be a "small-eddy theory" ([13, p. 208]) for turbulence generated mechanically and does not take proper account of the influence of the bigger eddies; as these large eddies are absent in the turbulent flow of the lower surface atmospheric boundary layer, some success attended the introduction of mixing-length concepts on account of the fact that momentum seems to be transferred mainly by smaller isotropic eddies (the same does not occur for heat transfer, for which some extraneous effect such as buoyancy enters).

However, across the whole depth of a real rotating atmospheric ABL, bigger non-isotropic vortices can be present (as well as wakes due to complexity of terrain, or large 2D coherent structures due to the Earth rotation). This fact can then support the presence of some transport processes in turbulent flow that is independent of the gradient of the entity being transferred, *i.e.* there might exist some "convective-like" processes as well as the usual diffusion mechanism.

Moreover, measurements of wind profiles near the ground indicate that ℓ is of the same order of magnitude as the height of observation, and therefore is not "small in the free-path sense". This fact too has the consequence that it may not be possible always to formulate a consistent theory of turbulent properties by using simply the down gradient approximation: there may be a term, or terms, depending on the transported variable and some mean velocity [2, 21].

In conclusion, our experiments highlighted that only the theoretical prediction of surface Rossby-number similarity in the atmospheric boundary layer is confirmed by experimental observation conducted in a rotating tank, while the accompanying Prandtl mixing length assumption is untenable.

6. – Conclusions

The experiment carried out in the rotating Laboratory of LEGI-Coriolis is described. The experiment was aimed to simulate a neutral boundary layer developed over flat boundary with different roughness lengths. Advanced measurement techniques, as PIV, were used in order to gather with high resolution data both in time and space. The results of the data analysis are presented in terms of mean flow and turbulence moments vertical profiles. The surface layer parameter and the boundary layer height were estimated in order to make the dynamical variable non-dimensional and to compare the different experiments with LES results. The experimental data underestimate the simulated ones. Nevertheless they show that the main characteristics of an ABL are capturated and, at least qualitatively reproduced. Concerning the diffusion coefficients, it has been shown that a partial surface Rossby number similarity exists on for $Z_R \geq 10\, Z_0$ due to the untenability of the Prandtl mixing length when non-isotropic big vortices exist in the rotating turbulent flow.

These conclusions suggested that the methodologies presented can be useful for comparing new turbulence parameterisation or more sophisticated models and for assessing their ability to reproduce the main features of the boundary layer. This is particularly interesting due to the possibility of the experimental facility to account for rotation.

* * *

The authors wish to thank D. Bertoni, R. Forza and S. Viboud for their skilful technical assistance before and during the experimental runs. This work has been carried out in the frame of the EU Program "Transnational Access to major Research Infrastructures".

REFERENCES

[1] Canuto V. M., Cheng Y. and Howard A., *J. Atmos. Sci.*, **58** (2002) 1169.
[2] Ferrero E. and Racca M., *J. Atmos. Sci.*, **61** (2004) 1434.
[3] Zeman O. and Jensen N. O., *Q. J. R. Meteorol. Soc.*, **113** (2004) 5580.
[4] Snyder W. H., Khurshudyan L. H., Nekrasov I. V., Lawson R. E. and Thompson R. S., *Atmos. Environ. A*, **25** (1991) 1347.
[5] Ohba R., Hara T., Nakamura S., Ohya Y. and Uchida T., *Atmos. Environ.*, **36** (2002) 5697.
[6] Moeng C.-H. and Sullivan P. P., *J. Atmos. Sci.*, **51** (1994) 999.
[7] Rizza U., Gioia G., Mangia C. and Marra G. P., *Nuovo Cimento C*, **26** (2003) 297.
[8] Fincham A. M. and Spedding G. R., *Exp. Fluids*, **23** (1997) 449.
[9] Ferrero E., Longhetto A., Manfrin M., Montabone L., Mortarini L., Didelle H., Sommeria J., Giraud C., Bertoni D. and Forza R., *Proceedings of Physmod2003* (Firenze University Press) 2003, p. 143.
[10] Raffel M., Willert C. E. and Kompenhans J., *Particle Image Velocimetry, a Practical Guide* (Springer Verlag, Berlin Heidelberg) 1998.
[11] Fincham A. M. and Delerce G., *Exp. Fluids*, **29** (2000) S013.
[12] Deardorff J. W., *Bound.-Layer Meteorol.*, **18** (1980) 495.
[13] Stull R. B., *An Introduction to Boundary Layer Meteorology* (Kluwer Academic Publisher) 1988.
[14] Tennekes H., *Workshop on Micrometeorology*, edited by Haugen D. A. (Am. Meteorol. Soc.), 1973 p. 177.
[15] Yamada T., *J. Atmos. Sci.*, **33** (1976) 781.
[16] Clarke R. H., Dyer A. J., Brook R. R., Reid D. G. and Troup A. J., *The Wangara Experiment: Boundary Layer Data*, Div. of Meteor., Physics Tech. Paper N 19 (CSIRO), Australia (1971).
[17] Arya S. P. S., *J. Atmos. Sci.*, **32** (1975) 839.
[18] Nicholls S., Lemone M. A. and Sommeria G., *J. R. Meteorol. Soc.*, **108** (1982) 167.
[19] Grant A. L. M. and Whiteford R., *Boundary-Layer Meteorol.*, **36** (1987) 1.
[20] Wipperman F. and Yordanov D., *Beitr. Phys. Atm.*, **45** (1972) 66.
[21] Ferrero E., to be published in *Boundary-Layer Meteorol.*